Photoionization Broadening of the $1S-2S$ Transition in a Beam of Atomic Hydrogen

N. Kolachevsky[1,2], M. Haas[3], U. D. Jentschura[3], M. Herrmann[1], P. Fendel[1], M. Fischer[4], R. Holzwarth[1,4], Th. Udem[1], C. H. Keitel[3], and T. W. Hänsch[1,5]

[1] *Max–Planck–Institut für Quantenoptik, Hans–Kopfermann–Str. 1, 85748 Garching, Germany*

[2] *P.N. Lebedev Physics Institute, Leninsky prosp. 53, 119991 Moscow, Russia*

[3] *Max–Planck–Institut für Kernphysik, Saupfercheckweg 1, 69117 Heidelberg, Germany*

[4] *MenloSystems GmbH, Am Klopferspitz 19, 82152 Martinsried, Germany*

[5] *Ludwig–Maximilians–University, Munich, Germany*

We consider the excitation dynamics of the two-photon $1S-2S$ transition in a beam of atomic hydrogen by 243 nm laser radiation. Specifically, we study the impact of ionization damping on the transition line shape, caused by the possibility of ionization of the $2S$ level by the same laser field. Using a Monte-Carlo simulation, we calculate the line shape of the $1S-2S$ transition for the experimental geometry used in the two latest absolute frequency measurements (M. Niering *et al.*, PRL 84, 5496 (2000) and M. Fischer *et al.*, PRL 92, 230802 (2004)). The calculated line shift and line width are in excellent agreement with the experimentally observed values. From this comparison we can verify the values of the dynamic Stark shift coefficient for the $1S-2S$ transition for the first time on a level of 15%. We show that the ionization modifies the velocity distribution of the metastable atoms, the line shape of the $1S-2S$ transition, and has an influence on the derivation of its absolute frequency.

PACS numbers: 32.70.-n, 32.90.+a, 42.50.Hz

I. INTRODUCTION

High-precision spectroscopy of the $1S-2S$ transition in atomic hydrogen and deuterium provides an essential contribution to the determination of the Rydberg constant, the Lamb shift [1], the $2S$ hyperfine interval [2] as well as it allows to study nuclear properties of the proton [3] and the deuteron [4]. Recently it has been shown, that monitoring the absolute frequencies of narrow clock transitions (like the $1S-2S$ transition in hydrogen and quadrupole transitions in the Hg^+ and Yb^+ ions) over a prolonged time interval, opens an opportunity to set a stringent restriction on the possible slow variation of the fine structure constant [5, 6], testing very fundamental aspects of physics. This laboratory approach relies on the accuracy of the $1S-2S$ frequency measurement, which has now reached the level of 1.4×10^{-14}, but in principle has still room for improvement, since the Q-factor of this transition is about 2×10^{15}. The accuracy which is achievable experimentally is restricted by a number of systematic effects which shift the frequency and change the line shape. So a further increase of accuracy requires not only an upgrade of the experimental setup and an improvement of the signal-to-noise ratio, but also a tighter control of the systematic effects. Among these, the dynamic Stark shift, the second order Doppler effect and the time-of-flight (TOF) broadening have been considered as the most important issues until recently.

In this article, we analyze how the presence of ionization losses of the $2S$ state via the absorption of 243 nm photons contributes to the line shape of the $1S-2S$ transition in the experimental configuration used for the most recent absolute frequency measurement [5, 7]. Comparing the experimentally obtained intensity-dependent line width and frequency shift of the $1S-2S$ transition with results of a numerical simulation, we can also indirectly validate a number of atomic parameters like the two-photon transition matrix element, the AC Stark shift coefficient and the ionization coefficient, which were recently re-derived in a unified formalism [8]. In addition, Monte Carlo simulations allow to study systematic effects which are difficult to quantify experimentally. From this we gain new insights on the origin of the scatter in the $1S-2S$ absolute frequency data observed in the experiments of 1999 and 2003 [5, 7].

The article is organized as follows: In Sec. II, we describe in brief the experimental apparatus emphasizing points important for the current analysis, while the numerical model is given in Sec. III. We analyze the results in Sec. IV, followed by the conclusions.

II. EXPERIMENTAL SETUP

The basic experimental setup used for the spectroscopy of the $1S-2S$ transition in a cold beam of atomic hydrogen is described in detail in [9]. In this section we will focus on a description of the apparatus depicting the main features necessary for the current analysis and will present the relevant experimental results.

The dipole-forbidden $1S-2S$ transition is excited by means of a Doppler-free two-photon driving scheme in counter-propagating waves of equal frequencies. The necessary 243 nm radiation is produced by doubling the cw light emitted by a 486 nm dye laser in a β-barium borate crystal. The laser is stabilized to an external ultra-stable

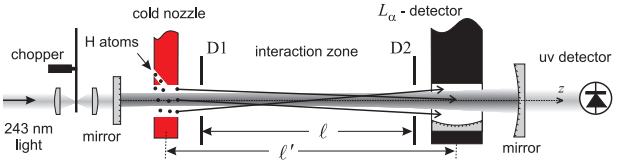

FIG. 1: Excitation of cold hydrogen atoms by 243 nm light in the enhancement cavity. Atoms escaping the cold nozzle are collimated by two diaphragms D1 and D2 before entering the detection zone. All parts except the chopper assembly and the uv photodiode are placed in vacuum of 10^{-7}–10^{-6} mbar. The diameters of the nozzle and the diaphragms are drawn not to scale and are much smaller as suggested by this graph.

cavity and has a spectral line width of about 60 Hz while the drift of the laser frequency is less than 0.5 Hz/s [5]. The frequency of the 486 nm laser is measured using the frequency comb technique [5, 10] which is described in detail in [11].

To efficiently excite the $1S-2S$ transition in atomic hydrogen we enhance the 243 nm radiation in a linear cavity consisting of a plane incoupling mirror (transmission $T_1 = 2.4 \times 10^{-2}$) and a concave outcoupling mirror (radius $R = -4$ m, $T_2 = 1.36 \times 10^{-4}$) separated by a distance of 29 cm as depicted in Fig. 1. The cavity loss is dominated by the diaphragms D1 and D2 that partially touch the laser mode so that the input coupling mirror roughly corresponds to impendence matching condition. The radiation leaking out of the cavity is monitored by a silicon photodiode which is periodically calibrated by a power meter (Fieldmaster, Coherent Inc.). The photodiode readout has been averaged over one second which is the laser dwelling time when recording the spectra. Dividing the photodiode readout by the transmission of the outcoupler T_2 we get the total power circulating in the enhancement cavity per direction. The averaged power is recorded for each measured spectrum.

Atoms produced in the microwave gas discharge escape a cold nozzle ($T \simeq 5$ K) of 1.2 mm in diameter and enter the interaction zone of length $\ell' = 15.0$ cm, restricted by two diaphragms D1 and D2 of respective diameters $2r_{\rm D1} = 1.3$ mm and $2r_{\rm D2} = 1.4$ mm separated by $\ell = 13.6$ cm. During the flight through the Gaussian profile of the cavity TEM_{00} mode, a part of the atomic hydrogen is excited to the metastable $2S$ state. Excited atoms are detected by quenching in a dc electric field through the release of a Lyman-alpha photon [9].

To set an upper limit for the velocity of the atoms that contribute to the signal and thus to reduce the influence of the velocity-dependent systematic effects, a time-of-flight detection technique [5, 9] is used. All atoms with velocities higher than $v_{\rm max}$ escape the detection zone before the start of the detection and the contribution of these atoms is excluded from the resulting time-delayed spectrum. The cut-off velocity is defined as $v_{\rm max} = \ell'/\Delta\tau$, where $\Delta\tau$ is a delay between closing of the 243 nm laser light and the start of detection.

The 486 nm laser is scanned stepwise across the resonance and for each laser frequency a multichannel scaler records the number of detected Lyman-α photons for 12 different delays $\Delta\tau_i = 10,\ 210,\ 410,\ \ldots,\ 2210\ \mu s$ in the corresponding time windows $\{\Delta\tau,\ 3\ \mathrm{ms}\}$.

Using this detection technique we simultaneously record 12 lines, each containing the contributions of atoms in the respective velocity range $0 < v < v_{\rm max}(\Delta\tau_i)$ $(i = 1, \ldots, 12)$, selected from the same initial velocity distribution $f(v)$. As follows from [12], the velocity distribution in a one-dimensional thermal atomic beam effusing from thermalized gas volume through a hole in a thin wall is given by:

$$f(v) \propto (v/v_0)^3 \exp[-(v/v_0)^2]\,, \qquad (1)$$

where $v_0 = \sqrt{2k_BT/m_{\rm H}}$ is the most probable thermal velocity for a given temperature T and $m_{\rm H}$ is the mass of hydrogen atom. As discussed in Ref. [12] and references therein, expression (1) is valid for perfectly collimated beams and should be further modified in other cases also because the thin wall assumption is not fulfilled in our case. The collimation angle of the atomic beam in our experiment is about 0.01 which justifies the use of the mentioned approximation.The impact of this approximation on the $1S-2S$ frequency shift will be discussed in Section IV C.

The increase of the delay $\Delta\tau$ reduces the maximum velocity $v_{\rm max}(\Delta\tau)$ of atoms contributing to the signal and decreases the Lyman-α count rate. Correspondingly, the contributions of the time-of-flight broadening and the second-order Doppler effect are reduced, which in turn leads to a narrowing and a symmetrization of the $1S-2S$ transition line shape. Hence, at the cost of a lower signal-to-noise ratio, lines with lower systematics are recorded. Using this experimental approach and the line-shape model [9] one can correct for the second order Doppler effect which is necessary for the accurate determination of the absolute $1S-2S$ transition frequency.

In this paper we will study three types of intensity related line broadening effects: Because the $2S$ state is close enough to the continuum that a single additional 243 nm photon is sufficient to ionize the hydrogen atom reducing the effective interaction time. In addition the spatially dependent AC Stark shift and the usual power broadening caused by Rabi flopping are present.

For simplicity, we will analyze only hydrogen lines recorded at a particular delay, $\Delta\tau = 1210\ \mu$s which corresponds to $v_{\rm max} \simeq 120$ m/s: this is a compromise between simple line shape and sufficient signal-to-noise ratio. At this delay the line shape can be well approximated by a Lorentzian and the maximum second-order Doppler effect does not exceed 200 Hz in modulus, the typical line width being 1-2 kHz at 121 nm. Therefore we consider contributions to the width of a Lorentzian line, which provides a much clearer insight into the nature of the different broadenings than the complete line shape model for all $\Delta\tau$.

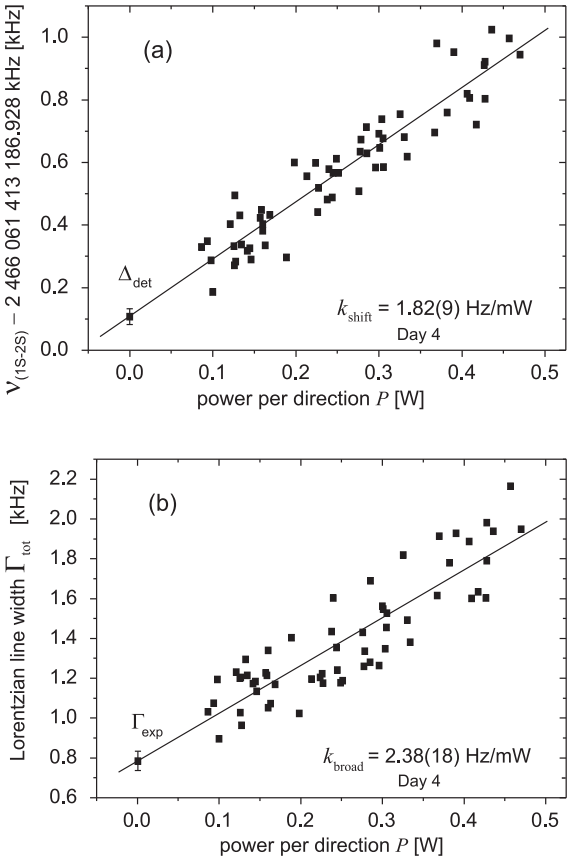

FIG. 2: Results from 59 line scans: (a) center frequencies and (b) line widths (FWHM) both derived from Lorentzian fits versus the excitation power circulating in the cavity per direction, P. The power of 1 W per direction corresponds to a total on-axis focal intensity of 16 MW/m^2 averaged over one wavelength of the standing wave.

To correct for another important systematic effect, the dynamic Stark shift, we recorded a number of $1S-2S$ spectra at different excitation powers during each day of measurement [5]. Here we use the same set of data for the analysis.

All lines recorded at $\Delta\tau = 1210$ μs have been fitted by Lorentzian functions and then the absolute frequencies of the line centers ν_{1S-2S} and line widths Γ_{tot} were plotted versus the excitation light power P (per direction). The results for the data set recorded on one of the days of measurement and the linear extrapolation to zero intensity are presented in Fig. 2 as an example.

The intensity-dependent line shift $\nu_{1S-2S}(P)$ is mainly caused by the dynamic Stark shift [8] with small contributions of velocity-selective ionization. As in Refs. [5, 7] we fit the data with a linear function (since for low intensities the AC Stark shift for $1S-2S$ transition is proportional to the intensity), but instead of extracting just the absolute frequency at zero power we also determine the slope of the fit, k_{shift}, as shown in the figure. Correspondingly, we consider the slope of the linear fit of the $\Gamma_{tot}(P)$ dependence and call it k_{broad}. It will be shown in the following that this coefficient is formed by three important contributions, namely power broadening, inhomogeneous AC Stark shift in a Gaussian beam profile and the influence of the ionization of the $2S$ level.

In the next section we will analyze the structure of these coefficients by the help of a numerical analysis performed for an ensemble of hydrogen atoms excited in the given experimental geometry.

III. EXCITATION OF A BEAM OF ATOMIC HYDROGEN IN THE PRESENCE OF IONIZATION

The calculation of the $2S$ excitation dynamics is based on the equations of motion for the matrix elements of the density operator ρ' in the rotating wave approximation [8]. The laser field of angular frequency $\omega_L \simeq 2\pi \times 1233$ THz, corresponding to $\lambda = 243$ nm, and intensity I excites the two-photon transition between the ground state $|g\rangle$ $(1S)$ and the excited state $|e\rangle$ $(2S)$. The frequency detuning is defined to be the difference between the doubled laser frequency and the resonance frequency $\Delta\omega = 2\omega_L - \omega'_{eg}$, where $\hbar\omega'_{eg}$ is the energy difference between the $1S$ and $2S$ states of a perturbed atom (see Eq. (3)), ignoring the the hyperfine structure [2].

In the experiment, the excitation field intensity I depends on the position inside the excitation region, because the laser profile is of Gaussian type. The fact that each atom flies along a certain trajectory with an individual speed through this intensity profile, renders the intensity a time dependent quantity $I(t)$ in the frame of the travelling atom. Because the dynamic Stark effect is proportional to the intensity, also the total detuning as measured by the atom, is a function of time, $\Delta\omega(t)$. In addition the upper state $|e\rangle$ decays to the continuum due to photoionization with a time-dependent rate proportional to the laser intensity. One can write the equations of motion for the density matrix, neglecting spontaneous decay of the $2S$ state [8]. After factoring out the fast optical oscillations from the components of the density matrix ρ via $\rho' = \rho\exp(-2i\omega_L t)$ we obtain the two-photon Bloch equations:

$$\frac{\partial}{\partial t}\rho'_{gg}(t) = -\Omega(t)\,\mathrm{Im}(\rho'_{ge}(t)), \tag{2a}$$

$$\frac{\partial}{\partial t}\rho'_{ge}(t) = -\mathrm{i}\,\Delta\omega(t)\rho'_{ge}(t) + \mathrm{i}\frac{\Omega(t)}{2}(\rho'_{gg}(t) - \rho'_{ee}(t)) - \frac{\gamma_\mathrm{i}(t)}{2}\rho'_{ge}(t), \tag{2b}$$

$$\frac{\partial}{\partial t}\rho'_{ee}(t) = \Omega(t)\mathrm{Im}(\rho'_{ge}(t)) - \gamma_\mathrm{i}(t)\rho'_{ee}(t), \tag{2c}$$

where the time-dependent two-photon Rabi frequency is $\Omega(t) = 2(2\pi\beta_{ge})(m_e/\mu)^3 I(t)$. Here m_e is the electron mass, μ the reduced mass, and the value of β_{ge} is taken from [8]: $\beta_{ge} = 3.68111 \times 10^{-5}$ Hz(W/m^2)$^{-1}$

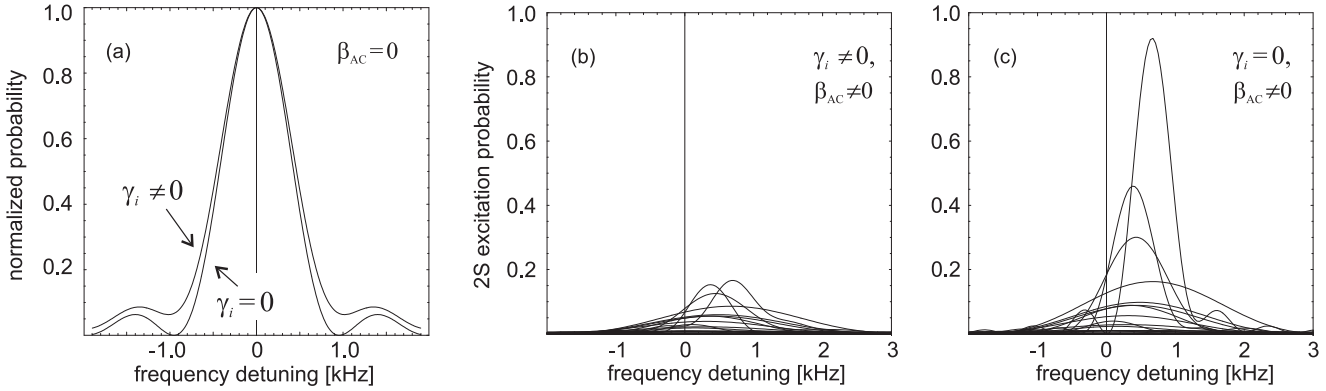

FIG. 3: (a) – normalized responses of a single atom illuminated by a 1 ms rectangular pulse with the intensity of $I = 4$ MW/m^2 with ionization channel ($\gamma_{\rm i} \neq 0$) and without it ($\gamma_{\rm i} = 0$). For simplicity, neither the AC Stark shift nor the Doppler effect are taken into account. (b), (c) – excitation probabilities for atoms flying along different random trajectories through the Gaussian intensity profile corresponding to $P = 300$ mW. (b) – calculations for 50 randomly chosen trajectories in presence of the ionization channel. (c) – calculation for the same ensemble of trajectories without ionization taken into account.

for the $1S-2S$ transition. In the same paper the ionization rate is given by $\gamma_{\rm i}(t) = 2\pi\beta_{\rm ioni}(e)(m_e/\mu)^3 I(t)$, where the ionization coefficient reads $\beta_{\rm ioni}(e) = 1.20208 \times 10^{-4}$ Hz $({\rm W/m^2})^{-1}$.

Experimentally an ensemble of atoms contributes to the signal, with each individual atom having a different speed and trajectory through the interaction zone. We take into account only those trajectories, which are confined by the diaphragms D1 and D2 (see Fig. 1). It is assumed, that the starting points on the diaphragm D1 and the exit points on the diaphragm D2 defining each trajectory are randomly and independently distributed over the corresponding diaphragm with constant area density. It means, that the angle $\varphi > 0$ between the cavity axis z and each individual trajectory is also randomly and uniformly distributed for $r_{\rm D1},\ r_{\rm D2} \ll \ell$: the atom can intersect the excitation light beam as well as fly parallel to its axis. The velocities are also chosen at random according to a Maxwellian distribution like in Eq. (1) at $T = 5$ K, as in the experiment the day-averaged readouts of the temperature sensor, placed on the cold nozzle, ranged between 4.95 K and 5.25 K.

After this longitudinal velocity seeding, all atoms which would reach the detector earlier than the time at which the delayed detection started (that is before $\Delta\tau = 1210$ μs), were rejected from the ensemble. For each remaining atom, one can then easily calculate the time-dependent intensity $I(t)$, as well as the total interaction time. The laser is modelled by a Gaussian beam profile with parameters defined by the experimental geometry. The radial intensity distribution is therefore given by $I(r) = (4P/\pi w^2)\exp[-2r^2/w^2]$, where $w^2 = w_0^2(1 + (z\lambda/\pi w_0^2)^2)$. The beam slightly diverges along the z-axis, and the beam waist on the incoupler plane equals $w_0 = 283$ μm. Here P is the power per direction, as used in Fig. 2.

It is necessary to point out, that atoms flying through a standing wave in the cavity interact with a highly inhomogeneous laser field consisting of nodes and maxima with the periodicity of 121.6 nm in z-direction. But even for a very slow atom travelling at a longitudinal velocity of $v = v_0/300 \simeq 1$ m/s, Eq. (1), the intensity will be modulated at a frequency of about 10 GHz, which is 6 orders of magnitude higher than the typical Rabi frequency Ω, which governs the population dynamics. Thus for the calculation of the density matrix elements, we can equivalently use a laser field with an averaged intensity, in a similar way as in applying the rotating wave approximation.

The general detuning $\Delta\omega(t)$ along the trajectory can now be expressed as

$$\begin{aligned}\Delta\omega(t) &= 2\omega_L - \omega'_{eg} = \\ &= 2\omega_L - \omega_{eg} + \frac{\omega_{ge}}{2}\left(\frac{v}{c}\right)^2 - 2\pi\,\beta_{\rm ac}\,I(t),\end{aligned} \tag{3}$$

where $\hbar\omega_{eg}$ is the energy between the unperturbed $1S$ and $2S$ states. The other summands take into account the second order Doppler effect and the intensity-dependent frequency shift caused by the real part of the dynamic Stark effect. In turn, the imaginary part of the dynamic Stark effect is related to ionization. According to [8], $\beta_{\rm ac} = [\beta_{\rm ac}(2S) - \beta_{\rm ac}(1S)](m_e/\mu)^3 = 1.66982\times10^{-4}$ Hz $({\rm W/m^2})^{-1}$.

The time evolution of Eqs. (2) for a specific atom and its corresponding interaction time is calculated numerically for each given laser frequency ω_L which is scanned stepwise across the resonance. The resulting value of ρ'_{ee} is stored together with ω_L to define the contribution of each individual atom to the line profile.

Fig. 3a illustrates the spectral response of a single atom at rest to the excitation with the rectangular pulse of 243 nm radiation. This case is analyzed in detail in [8]. One observes, that for moderate excitation intensities of a few MW/m^2 and for short interaction times less then 1 ms, the contribution of the ionization broadening to the total line width is practically negligible. Indeed, for

a 1 ms rectangular pulse of intensity $I = 4$ MW/m^2 the ionization broadening is a very small effect, though the ionization rate itself in this case equals $\gamma_{\rm i} = 480$ Hz.

Fig. 3b illustrates how individual atoms flying through the excitation region contribute to the observed line shape. Depending on the individual trajectory and the velocity of an atom it will be exposed to a time varying intensity. The figure shows the resulting individual line shapes, over which the detector integrates to yield the observed line profile. Note the variations in amplitude, shift and width of the individual lines due to varying speeds (second order Doppler shift), interaction times (excitation and ionization probability, TOF broadening) and sampled intensities (excitation and ionization probability, AC Stark shift, power broadening).

In contrast to the physical case given in Fig. 3b with all effects taken into account, Fig. 3c shows the excitation probabilities for *the same ensemble* of 50 trajectories calculated without ionization. Apparently the ionization preferably removes the slow atoms from the initial distribution, because they have more time to interact with the field. But these atoms would have contributed the strongest and the narrowest spectral lines to the resulting collective spectrum if no ionization had taken place. As a result, the detected line becomes weaker and broader.

In the results section we will discuss the simulated line profiles in more detail and compare the results with experimental data.

To perform the described Monte-Carlo simulation we used the package "Mathematica 5" [13]. The simulation has shown good convergence and an arbitrary ensemble of 10 000 atoms has been used to calculate each transition line shape. The input parameters used by the program can be divided into four groups: (i) atomic structure, (ii) geometric parameters (w_0, $r_{\rm D1}$, $r_{\rm D2}$, ℓ, ℓ', nozzle radius), (iii) experimental conditions (P, T, $\Delta\tau$) and (iv) two program switches which allowed to artificially set $\gamma_i = 0$ (no ionization) or $\beta_{\rm ac} = 0$ (no AC Stark shift). The last option allows to analyze separately the contributions of ionization, AC stark shift and power broadening to the line shape.

Including all contributions to $\rho'_{ee}(\Delta\omega_L)$, we obtain the simulated line shape, which we fit with a Lorentzian profile exactly like in the evaluation of the experimental data for the purpose of this study. In our simulations, we varied the excitation power up to $P = 1.2$ W per direction which covers and exceeds the whole experimental range.

IV. RESULTS

In this section the results of the numerical simulation will be compared with experimental results obtained in the measurement [5]. We will analyze the frequency shift and the line shape of the $1S-2S$ transition and discuss possible origins of the excess data scattering observed in the frequency measurement experiments.

We would like to point out here, that both the frequency shift and the line broadening are *very small* effects of the order of 10^{-12} compared to the optical carrier frequency. Only the improvements of the laser stability and the narrowing of its spectral line width along with an improved absolute frequency measurement have made it possible for the first time to perform a *quantitative* analysis of the line shift and especially of the line broadening as a function of excitation intensity.

Figure 4 illustrates the results of the different simulations (a, b) and their comparison with experimental observations (c, d). To evaluate the uncertainty of the simulation for 10 000 atoms due to the random elements of the simulation, we performed the simulation for 3 different arbitrary ensembles of atoms for the same input program parameters. The variation is on the level of few per cent which is sufficient for this analysis.

A. Line Center Shift

As follows from Fig. 4a, the main origin of the frequency shift is the AC Stark shift. The physical case is depicted in a solid curve ($\gamma_{\rm i} \neq 0,\ \beta_{\rm ac} \neq 0$). The line shift reveals an observable non-linearity at higher powers. It could be explained by the following contributions: (i) the inhomogeneous AC Stark shift, (ii) the influence of ionization and (iii) the saturation of the transition. In the current analysis we took the non-linearity into account by fitting the simulations in Fig. 4a with a parabolic function.

For comparison with the full treatment, we performed the same set of calculations for three non-physical cases: with the ionization channel switched off ($\gamma_{\rm i} = 0,\ \beta_{\rm ac} \neq 0$), the AC Stark shift is switched off ($\gamma_{\rm i} \neq 0,\ \beta_{\rm ac} = 0$), and both these effects are switched off ($\gamma_{\rm i} = 0,\ \beta_{\rm ac} = 0$). We see, that the main contribution to the frequency shift is due to the real part of the dynamic Stark shift. The ionization, which reduces the number of atoms undergoing the highest perturbation in the intensive laser field. It also influences the frequency shift, but only if the dynamic Stark shift is present as well. All data sets in Fig. 4a converge at zero power to the same value of $-20(1)$ Hz which corresponds to the mean second order Doppler shift for the given beam temperature of $T = 5$ K and the delay time $\Delta\tau = 1210$ μs. This value is considerably smaller than the maximal shift of -200 Hz calculated for $v_{\rm max}(\Delta\tau)$. This difference is caused by the fact that the velocity distribution of atoms which contribute to the signal $f'(v)$ is different from the velocity distribution of atoms in the beam $f(v)$: neglecting additional losses it is given by

$$\begin{aligned} f'(v) &\propto f(v)(1 - v/v_{\rm max}(\Delta\tau)), \quad v < v_{\rm max}, \\ f'(v) &= 0, \qquad\qquad\qquad\qquad\quad v \geq v_{\rm max}. \end{aligned} \tag{4}$$

Consequently, the Doppler correction must take this weighting into account. A further correction to the effective second order Doppler effect is invoked by the preferred removal of slow atoms. As seen in Fig.4a (for

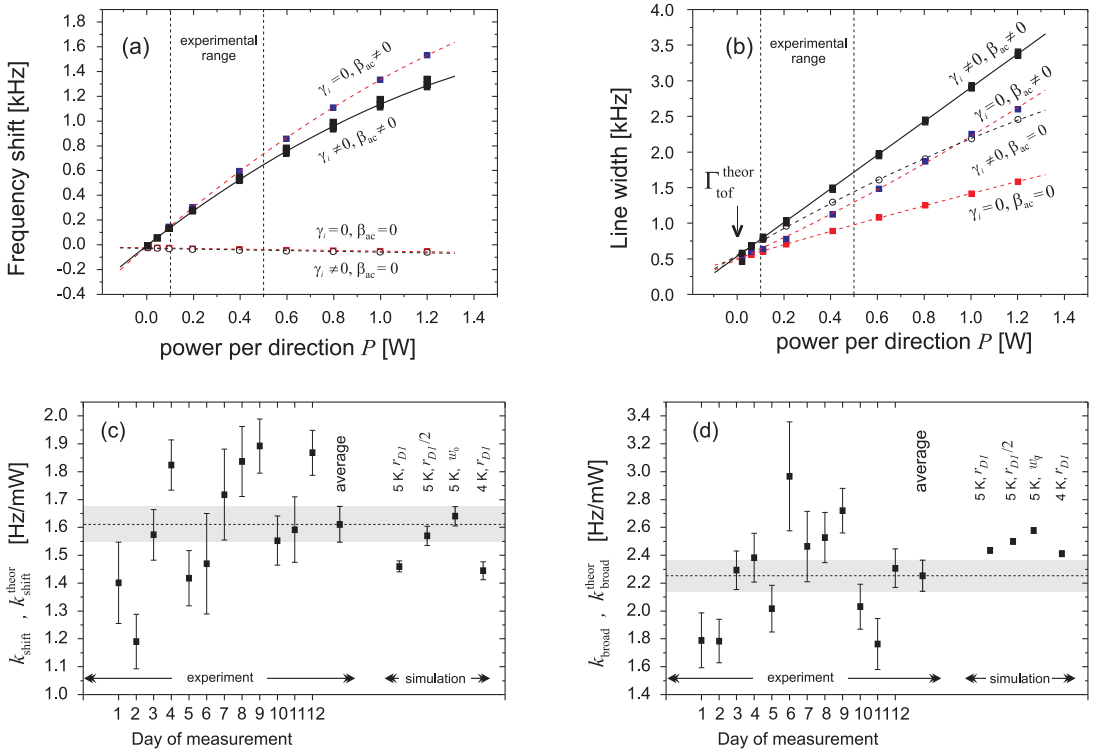

FIG. 4: Simulated dependencies of the frequency shift (a) and the line width (b) of the $1S-2S$ transition vs. excitation power per direction, P and a detection delayed by $\Delta\tau = 1210$ μs. The set of data marked $\beta_{\rm ac} \neq 0$, $\gamma_{\rm i} \neq 0$ corresponds to the physical case. The other simulations clarify the separate contributions of ionization, inhomogeneous AC Stark shift and power broadening (e.g. the data set with $\gamma_{\rm i} = 0$, $\beta_{\rm AC} = 0$ in (b) corresponds to pure power broadening). Note that the contributions cannot be added in any simple algebraic way. The data sets are fitted by parabolic functions. On the left side of (c) and (d) the the day-averaged values of $k_{\rm shift}$ and $k_{\rm broad}$ with corresponding uncertainties are presented. The total 12-day average of the data is indicated by the dashed lines and the gray bars for the uncertainties. Simulations for two different beam temperatures (5 K and 4 K) and for different radii of the entrance diaphragm D1 ($r_{\rm D1}$, $r_{\rm D1}/2$ and w_0) are presented on the right part of the lower plots.

$\gamma_i \neq 0$, $\beta_{\rm ac} = 0$) this preference and thus the associated shift is vastly independent of laser power for our experimental conditions. As it is impossible in our experiment to measure the Stark coefficients $\beta_{\rm ac}$ and $\beta_{\rm ioni}$ separately, we analyze the values which can be derived both from the experiment and our numerical analysis, namely the slopes $k_{\rm shift}$ and $k_{\rm broad}$ of the power dependencies given in Fig. 2 and Figs. 4a, b.

On the experimental side, we derive these values for each of the 12 days of measurement exactly in the same way as depicted in Fig. 2. The results for each day are presented in Figs. 4 c,d. One observes a significant scatter of the day-to-day data, with $\chi^2_r \simeq 3$ (the reduced χ^2 or Birge ratio [14]), which could be partly ascribed to errors on the power axis, coming from both the calibration of the photodiode measuring the 243 nm power and from temporal variations of the transmittance of the curved mirror in Fig. 1. Therefore we average these data without taking into account the individual uncertainties and obtain $k_{\rm shift} = 1.61(6)$ Hz/mW and $k_{\rm broad} = 2.25(11)$ Hz/mW.

Extracting the coefficient $k_{\rm shift}$ from the results of the numerical analysis, depicted in Fig. 4a, is not straightforward, since the curve for the shift of the line center are not linear and therefore $k_{\rm shift}$ is not strictly defined. However, since the scatter in the experimental data is larger than the calculated nonlinearities, it is enough on the present level of accuracy to replace the parabolic fit by a linear fit in the case of the frequency shift-intensity dependence ($k_{\rm shift}$), in order to evaluate the results in the same way as in the experiment. To reduce the error introduced by this procedure, we restrict the data points taken into account by the fit to those which fall into the experimental range of powers: 0.1 W $< P <$ 0.5 W. The value resulting from the Monte Carlo analysis is denoted as $k^{\rm theor}_{\rm shift}$ in analogy to the notation in Fig. 1.

To test the sensitivity of the model to the experimental conditions and to evaluate the corresponding uncertainties we also performed a set of simulations for different beam temperatures, varying between 4 K and 6 K, slightly different interaction lengths and a reduced radius r_1 of the diaphragm D1. All these tests show a low sensitivity of results to these parameters which allows to compare them with the experimental data. We have

performed calculations of $k_{\rm shift}^{\rm theor}$ for different realistic experimental parameters. The results of four selected cases are given in Fig. 4c: with an atomic beam temperature of 4 and 5 Kelvin and for a diaphragm size matched and centered to the laser beam to simulate the nozzle covered with a molecular hydrogen film.

The last case corresponds to a possible situation, where a film of molecular hydrogen symmetrically covers the nozzle from inside in such a way that the nozzle radius equals either $r_{\rm D1}/2$ or $w_0 = 283$ μm (the film eventually touches the laser beam). The frozen nozzle radially restricts the atomic trajectories on the entrance to the interaction zone, which results in changing the intensity profiles. The growth of the H_2 film was a characteristic feature of the hydrogen spectrometer working at the lowest beam temperature. The measurement cycle lasted about 15 min, after which the nozzle was heated to 20 K to melt the film.

Comparing the averaged value $k_{\rm shift}$ with the results of the numerical simulation, we can establish an agreement on the level of about 15% uncertainty with respect to the absolute values. As follows from the previous analysis, the intensity-dependent frequency shift is mainly caused by the AC Stark shift which contributes to the general detuning (3). Using the linearity of the effect at low powers one can conclude, that this analysis allows to verify $\beta_{\rm ac}$ at the same confidence level of 15% and therefore we can experimentally verify the results of the calculations of $\beta_{\rm ac} = \beta_{\rm ac}(2S) - \beta_{\rm ac}(1S)$ presented in [8].

B. Line Width

The analysis of the line width is more complicated in comparison with the analysis of the frequency shift since a number of different effects contribute significantly to the line broadening. The line width consists of intensity-independent and intensity-dependent parts. The intensity-independent part includes the laser spectral line width and the time-of-flight broadening, while such effects as power broadening, inhomogeneous AC Stark broadening and ionization broadening contribute to the latter part. In addition, temporal intensity fluctuations of the laser radiation in the excitation region also induce an additional intensity-dependent broadening due to the variable Stark shift. Thus, assuming for simplicity the Lorentzian profiles, one can write:

$$\Gamma_{\rm tot}(P) = \Gamma(P) + \Gamma_{\rm tof} + 4\,\Gamma_{\rm laser}\,, \qquad (5)$$

where $\Gamma_{\rm tot}(P)$ is the total line width, $\Gamma_{\rm tof}$ is the contribution of the time-of-flight broadening, and $\Gamma(P)$ includes all intensity-dependent effects with $\Gamma(0) = 0$. The laser line width $\Gamma_{\rm laser}$ carries a factor of 4 because we measure it at 486 nm whereas all other transition frequencies correspond to 121 nm. It has been shown experimentally, that the spectral line width of our laser system doubles for the frequency doubling process. We understand that each of the contributions listed above has a complex spectral shape which can significantly differ from Lorentzian and the expression (5) can be used only for rough estimations. Still, the simulations show that in our case the time-of-flight broadening has near-to-Lorentzian spectral line shape while heterodyne experiments indicate the same for the spectral line of our laser system.

As is evident from Fig. 4b, the intensity-dependent part of the line width is formed by three different processes: (i) the power broadening, (ii) the inhomogeneous AC Stark shift in the laser beam profile and (iii) the ionization of the $2S$ state. The pure power broadening corresponds to the case ($\gamma_{\rm i} = 0,\ \beta_{\rm ac} = 0$) and is due to Rabi flopping between the ground and the excited states, effectively reducing the lifetime of the population in the excited $2S$ state. The inhomogeneous AC Stark shift in the case ($\gamma_{\rm i} = 0,\ \beta_{\rm ac} \neq 0$) originates from a Gaussian intensity profile in the excitation region. The last significant broadening comes from ionization which contributes in a highly nontrivial way illustrated in Figs. 3b,c.

The excessive loss of slow atoms has been taken into account in the line form model [7, 9] as an empirical modification of the low-velocity wing of the Maxwellian v^3-dependency in Eq. (1). There it was assumed that the slow atoms are missing from the beam because of collisions with the fast atoms (Zacharias effect). However, now we conclude that no such mechanism is necessary to fit our data and the selective ionization is the most significant effect responsible for this loss. Strictly speaking, one deals with three distinct velocity distributions: (i) the atoms emerging from the nozzle, (ii) the detected $2S$ atoms, and (iii) the ground state atoms. Whereas the first distribution is assumed to be Maxwellian (Eq. (1)), the second is relevant for determining the line shape.

To compare with the experimental results, we also evaluated the contribution of the temporal intensity fluctuations. In principle, this effect is equivalent to the considered inhomogeneous AC Stark shift, but integrated over time, not space. In the experiment, we observed fast intensity fluctuations on the level of $\pm 5\%$ during the excitation cycle. We embedded this process into the simulation by adding white noise with a 5% band to $I(t)$. The effect lies within the uncertainty of the calculations for the given number of atoms used in the simulation.

For the line width as a function of laser power, the slope is derived from the fit similar to the case of Fig. 4a. The value resulting from the Monte Carlo analysis is denoted as $k_{\rm broad}^{\rm theor}$. The line width, extrapolated to zero power, is $\Gamma_{\rm tof}^{\rm theor} = 550(5)$ Hz which corresponds to the theoretical value for the averaged time-of-flight broadening for the given delay $\tau = 1210$ μs in the absence of other broadening contributions (Fig 4b).

The value $k_{\rm broad}$ can be tested in the same way as $k_{\rm shift}$ with an uncertainty of 18% (see Fig. 4d). Due to the complex structure of this value and the number of contributions of different nature which add up to the total line broadening, it is impossible to disentangle them

and to set separate restrictions on the transition matrix element and the ionization cross-section. Nevertheless, if we switch off any of the important broadening mechanisms, as illustrated in Fig. 4, the simulation will no longer agree so well with the experimental observation. This means that both the calculations performed in [8] as well as the current analysis adequately describes the excitation dynamics of the hydrogen atom in the presence of photoionization.

For consistency of our analysis, we also performed an evaluation of the laser line width $\Gamma_{\rm laser}$. Studies of the spectral laser line width at 486 nm, based on the investigation of beat signals, resulted in a value of 60 Hz [15]. In the framework of this paper, we can make an estimate of its spectral line width with a different, indirect method. To this end, we compare the calculated line width at zero laser power $\Gamma_{\rm tof}^{\rm theor}$ with the experimentally observed line width $\Gamma_{\rm exp}$, where the latter is obtained by averaging the extrapolated day values for the line width similar to Fig. 2b, resulting in $\Gamma_{\rm exp} = 775(20)$ Hz. From Eq. (5) we obtain $\Gamma_{\rm laser} = 56(5)$ Hz, which is consistent with the previous independent measurement [15]. The splitting of the $(1S,\, F=1,\, m_F=\pm1) \rightarrow (2S,\, F'=1,\, m'_F=m_F)$ magnetic components is negligible in the experiment.

An attempt to directly evaluate the expected Lyman-α count rate in the given experimental geometry and thus test the theoretical values more directly fails due to the large uncertainties in the beam density, the fraction of atomic hydrogen in it and the detection efficiency. The presented indirect analysis happens to be much more sensitive to the absolute values of the transition matrix elements and the ionization cross section than the direct evaluations.

C. Impact on the $1S-2S$ Absolute Frequency Determination

At the end of this section we discuss the conclusions of the current analysis regarding the absolute frequency measurement of the $1S-2S$ transition in atomic hydrogen.

First of all, we want to point out the non-linearity of the frequency shift of the line center as a function of the laser power (Fig. 4a). Our analysis shows, that our previous linear fit leads to an error of 10-20 Hz in the determination of the absolute $1S-2S$ frequency $\omega_{ge}/2\pi$, if we restrict ourselves to the experimental range of powers (0.1 W $< P <$ 0.5 W). This does not contradict the uncertainty of the line shape model of 20 Hz given in [9]. Moreover, in the derivation of the possible small temporal drift of the $1S-2S$ frequency [5] this error cancels out. Still, for a further improvement of the $1S-2S$ frequency measurement it is highly desirable to reduce the laser intensity and thus reduce the error and the uncertainty of the extrapolation.

Secondly, the calculations show, that due to the photoionization, the velocity distribution of atoms escaping the nozzle significantly differs from the distribution of atoms contributing to the signal. For the correction of the second order Doppler effect it is more physical to model the initial velocity distribution in the nozzle by a Maxwellian distribution (see Eq. (1)), which is dynamically modified by the ionization process of atoms with long interaction times, instead of modelling an effective velocity distribution at the detector. On the other hand, the magnitude of the Doppler effect, which has been one of the biggest concerns in the last measurements [5, 7] is already on the level of -20 Hz for a delay time of $\Delta\tau = 1210$ μs. This opens an opportunity to use a simplified line shape model to correct for this effect.

We have performed an evaluation of the whole data set obtained in 2003 measurement [5] using such a simplified approach. The $1S-2S$ spectral lines detected with the delays $\Delta\tau > 1210$ μs have been fitted by Lorentzian functions. The frequencies of the line centers have been corrected for the second-order Doppler effect by adding the calculated frequency shift. The result of this analysis was consistent with the result of the full line shape model [9] within the uncertainty of the model. The shift should be sensitive to the initial velocity distribution which can differ from (1) due to e.g. geometrical factors, unperfect thermalization or collisions. The delayed detection modifying the velocity distribution (5) drastically reduces the mean Doppler shift as well as its sensitivity to the initial distribution. We tested numerically, that the substitution of the v^3 dependency (1) by v^4 results in a mean Doppler shift of -23 Hz for $\Delta\tau = 1210$ μs, which is only 3 Hz aside the previous value of -20 Hz. The difference decreases for increasing $\Delta\tau$ and the corresponding uncertainty in the determination the $1S-2S$ frequency can be reduced to a few hertz. Thus, using such a simplified model we can correct the second-order order Doppler effect with an uncertainty on the level of a few parts in 10^{15}.

The last point concerns the influence of the freezing nozzle on the observed absorption line centers, and resulting effects on the absolute frequency, which is obtained by the extrapolation of these line centers to zero laser power. Since the nozzle temperature is lower than its melting point of 14 K, molecular hydrogen effectively freezes on the nozzle walls and reduces its diameter. In the experiment, we had to melt molecular hydrogen approximately once per 20 min to avoid significant losses of laser power and atomic hydrogen flux in the 243 nm cavity. Our simulation allows for different spatial seedings of starting points of the atomic trajectories at the diaphragms, which can be used to model a reduced nozzle diameter or a misalignment of the cavity mode with respect to the atomic beam axis.

We have performed a simulation of a whole day of measurement recording the 1210 μs delayed spectra at 100 different intensities, while varying the nozzle radius randomly in the range from $r_{\rm D1}$ down to w_0. The resulting line center fits as a function of laser power per direction are shown in Fig. 5b. Figure 5a results from the same

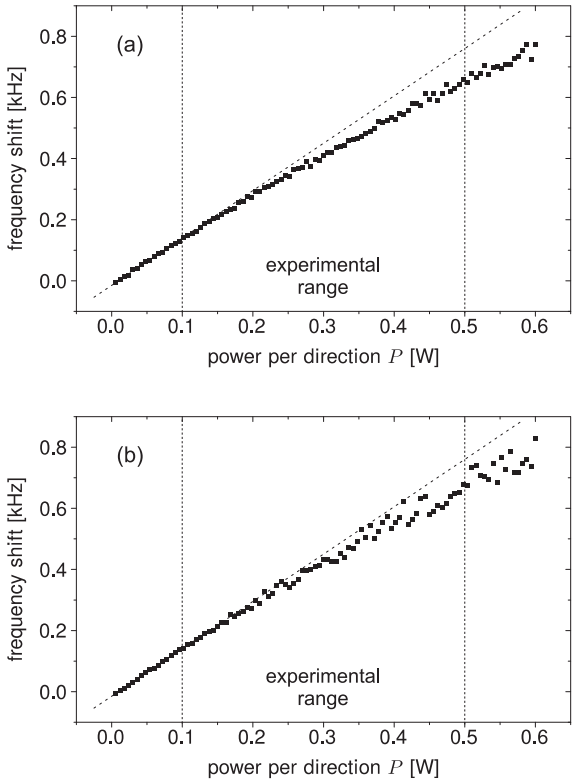

FIG. 5: Monte-Carlo simulation: (a) – the frequency of the $1S-2S$ transition vs. laser power for an ensemble of 10 000 atoms for the completely opened nozzle. The residual scatter of the data can be explained by the stochastic nature of the Monte-Carlo simulation. (b) – the same simulation, but the nozzle radius is randomly varied in the range $\{w_0, r_{\rm D1}\}$. We fit the data at low intensity limit by linear functions (dashed tilted lines) for visualization of non-linearity of the frequency shift.

simulation but with a permanently free nozzle. An uncontrolled freezing leads to an excess scatter of the line centers, increasing for larger exciting powers. Specifically, a smaller radius at the entrance diaphragm results in an upwards shift in line center frequency, the shift increasing with excitation power. This is consistent with the observation in Fig. 4c, where a small nozzle radius results in a larger value for $k_{\rm shift}$. As a result, a linear fit in the range of $0.1-0.5$ W and an extrapolation to zero intensity gives different values for the absolute frequency depending on the amount of nozzle freezing. Typically the scatter is on the level of a few tens of Hertz, which can only partly explain the scatter observed in the experiments [5, 7]. Other contributions can originate in uncertainties of the power axis and misalignment of the 243 nm enhancement cavity. In future measurements we will aim at increasing the nozzle diameter to avoid restriction of the atomic trajectories, working at lower excitation powers, and improving the stability of the enhancement cavity including power stabilization.

The beam nature of the $1S-2S$ spectroscopy of atomic hydrogen imposes certain restrictions on the experimental conditions like high intensity of the excitation field, impossibility of further cooling of the beam, short interaction time and freezing of the nozzle. The enumerated effects result in a number of systematic shifts and corresponding loss of accuracy. Note, that all optical spectroscopic experiments demonstrating the accuracy better than 10^{-14} deal with cold ions or atoms in traps (see e.g. [16, 17]). All the systematic shifts of the $1S-2S$ transition discussed in the paper would be significantly reduced or eliminated if the hydrogen atoms were slowed down by laser cooling or if one used hydrogen-like ions that could be held in a trap [18].

Based on considerations of this Section we can conclude, that perturbation of the mode of the enhancement cavity results in a frequency shift via the intensity related shift and broadenings. Though the cavity is not confocal which ensures the suppression factor over 500 for the $\rm TEM_{01}$ mode, the intra-cavity diaphragms can influence the structure of the $\rm TEM_{00}$ cavity mode. Monte-Carlo simulations performed for impure $\rm TEM_{00}$ mode shows that the results presented in the article remain valid if the power falling into the $\rm TEM_{01}$ mode does not exceed 5%. Thus, special attention should be paid for intensity stabilization, coupling and alignment of the cavity to avoid any additional non resonant light. After taking the issues discussed in the paper into account it seems realistic to reduce the uncertainty of the determination of the $1S-2S$ frequency to the level of a few parts in 10^{15}.

V. CONCLUSIONS

In this article we discussed the transient excitation dynamics of the $1S-2S$ transition of atomic hydrogen under irradiation of two counter-propagating 243 nm light beams. The main focus of the present analysis has been the inclusion of photoionization of the $2S$ state, power broadening and the inhomogeneous AC Stark in the quantum dynamics and the detailed study of their influence on the transition frequency and its line width.

Though photoionization would only insignificantly change the line width of each individual atom in the experimental range of excitation powers and interaction times in a laser field of constant intensity, the preferred ionization of slow $2S$ atoms results in a substantial broadening of the observed collective spectrum. The modelling shows, that the resulting intensity-dependent frequency shift is mainly caused by the dynamic Stark shift, while the intensity-dependent line broadening results from power broadening, the dynamic Stark shift in a spatially inhomogeneous laser field and the influence of photoionization.

For our simulation we used the values of the transition matrix elements, the dynamic Stark shift coefficients and the ionization rates re-derived in [8]. The results of the simulation show a fair agreement with the experimentally observed ones. We can confirm the value of the difference

of the dynamic Stark shift coefficients $\beta_{\rm ac}(2S) - \beta_{\rm ac}(1S)$ with an accuracy of 15% using the analysis of the $1S-2S$ frequency shift. The analysis of the line broadening also shows a good agreement with the experimental values within 18%. Due to a complex structure of the intensity-dependent line broadening it does not allow to make definite conclusions about the ionization coefficient, though indicating that our treatment of the excitation process in the thermal beam is correct.

The uncertainty of the determination of the $1S-2S$ frequency is determined not only by the experimental accuracy, but also by the uncertainty of the line shape model and the correction of the dynamic Stark shift. Taking photoionization into account allows to build a more accurate line shape model. Factors such as nonlinearity of the line shift and geometrical factors contribute on a level comparable in magnitude with the second order Doppler effect, which has been of major concern in previous studies [7, 9]. The Monte-Carlo approach presented in this paper allows to perform accurate quantitative evaluations of all these effects and make an accurate evaluation of the final uncertainty.

VI. ACKNOWLEDGEMENTS

N.K. acknowledges the support of RFBR (grants No. 04-02-17443, 05-02-16801), the Alexander von Humboldt Foundation, and thanks the scientific team of MPI für Kernphysik for the hospitality. U.D.J. acknowledges support from Deutsche Forschungsgemeinschaft (Heisenberg program).

[1] F. Biraben *et al.*, in: *The Hydrogen Atom. Precision Physics of Simple Atomic Systems*, ed. by S.G. Karshenboim, F. S. Pavone, G. F. Bassani, M. Inguscio, T.W. Hänsch (Springer, Berlin, Heidelberg 2001), 18-41.

[2] N. Kolachevsky, M. Fischer, S.G. Karshenboim, T.W. Hänsch *Phys. Rev. Lett.* **92**, 033003 (2004).

[3] Th. Udem, A. Huber, B. Gross, J. Reichert, T.W. Hänsch, *Phys. Rev. Lett.* **79**, 2646 (1997).

[4] A. Huber *et al.*, *Phys. Rev. Lett.* **80**, 468 (1998).

[5] M. Fischer *et al.*, *Phys. Rev. Lett.* **92**, 230802 (2004).

[6] E. Peik *et al.*, *Phys. Rev. Lett.* **93**, 170801 (2004).

[7] M. Niering *et al.*, *Phys. Rev. Lett.* **84**, 5496 (2000).

[8] M. Haas *et al.*, *Phys. Rev.* A, **73**, 052501, 2006.

[9] A. Huber, B. Gross, M. Weitz, and T. W. Hänsch, *Phys. Rev.* A **59**, 1844 (1999).

[10] M. Fischer *et al.* in: Lecture Notes in Physics: *Astrophysics, Clocks and Fundamental Constants*, S.G. Karshenboim and E. Peik eds., Springer Verlag Berlin, Heidelberg, vol. 648, 209 (2004).

[11] Th. Udem, R. Holzwarth, and T.W. Hänsch, *Nature*, **416**, 233 (2002).

[12] G. Scoles, D. Bassi, U. Buck, and D. Laine, *Atomic and Molecular Beam Methods*, Volume 1, Oxford University Press, New York (1988).

[13] S. Wolfram, "The Mathematica Book", 4th ed. (Wolfram Media/Cambrige University Press, 1999).

[14] R.T. Birge, *Phys. Rev.* **40**, 207 (1932).

[15] M. Fischer, N. Kolachevsky, S.G. Karshenboim, T.W. Hänsch, *Canadian Journal of Physics* **80**, 1225 (2002).

[16] L. Hollberg et al., *J. Phys. B: At. Mol. Opt. Phys.*, S469, **38** (2005).

[17] H.S. Margolis *et al.*, *Science* **19**, 1355 (2004).

[18] M. Herrmann, Th. Udem, C. Gohle, N. Kolachevsky, T.W. Hänsch, D. Leibfried, D. Wineland, M. Haas, U.D. Jentschura, and C.H. Keitel, *The $1S-2S$ transition in singly ionized helium: Feasibility of high precision spectroscopy in the XUV*, (unpublished).